nature COMMUNICATIONS

ARTICLE

Received 21 Jun 2016 | Accepted 17 Oct 2016 | Published 2 Dec 2016

DOI: 10.1038/ncomms13574 OPEN

A grand unified model for liganded gold clusters

Wen Wu Xu[1,2], Beien Zhu[1], Xiao Cheng Zeng[2,3] & Yi Gao[1,4]

A grand unified model (GUM) is developed to achieve fundamental understanding of rich structures of all 71 liganded gold clusters reported to date. Inspired by the quark model by which composite particles (for example, protons and neutrons) are formed by combining three quarks (or flavours), here gold atoms are assigned three 'flavours' (namely, bottom, middle and top) to represent three possible valence states. The 'composite particles' in GUM are categorized into two groups: variants of triangular elementary block $Au_3(2e)$ and tetrahedral elementary block $Au_4(2e)$, all satisfying the duet rule ($2e$) of the valence shell, akin to the octet rule in general chemistry. The elementary blocks, when packed together, form the cores of liganded gold clusters. With the GUM, structures of 71 liganded gold clusters and their growth mechanism can be deciphered altogether. Although GUM is a predictive heuristic and may not be necessarily reflective of the actual electronic structure, several highly stable liganded gold clusters are predicted, thereby offering GUM-guided synthesis of liganded gold clusters by design.

[1] Division of Interfacial Water and Key Laboratory of Interfacial Physics and Technology, Shanghai Institute of Applied Physics, Chinese Academy of Sciences, Shanghai, 201800 China. [2] Department of Chemistry, University of Nebraska-Lincoln, Lincoln, Nebraska 68588, USA. [3] Collaborative Innovation Center of Chemistry for Energy Materials, University of Science and Technology of China, Hefei, Anhui 230026, China. [4] Shanghai Science Research Center, Chinese Academy of Sciences, Shanghai 201204, China. Correspondence and requests for materials should be addressed to X.C.Z. (email: xzeng1@unl.edu) or to Y.G. (email: gaoyi@sinap.ac.cn).

Liganded gold clusters have attracted intensive interest over the past 10 years owing to their broad and practical applications in catalysis[1], electrochemistry[2], quantum electronics[3] and biomedicine[4]. A grand challenge to scientists in this field, however, is the precise determination of atomic structures of liganded gold clusters. To date, atomic structures of tens of liganded gold clusters have been determined via X-ray crystallography[5–63]. Nevertheless, these revelations appear serendipitous as the structural determination largely hinges on availability of single crystals for the liganded gold clusters. Although density-functional theory computation has been widely applied to predict the structures of many gold clusters[64–78], ultimate confirmation still requires X-ray crystallography measurements. Theoretical efforts have also been made in the past for more general unification models to comprehend stabilities of liganded gold clusters with apparently very different and seemingly unrelated complex structures. For example, Wade–Mingos counting rules[79,80] can provide a simple rationale of various shapes of 'electron-deficient' polyhedral clusters in terms of the number of skeletal electron pairs, particularly for borane and carborane clusters. However, few gold clusters can be rationalized by the Wade–Mingos counting rules[81], especially for the gold clusters with a high number of interstitial atoms, whose structures have been precisely resolved[60,61]. The superatom complex (SAC) model proposed by Walter *et al.*[82] suggests that the high stability of several spherical-like ligand-protected gold clusters[26,55,60] is due largely to the strong electron shell closures, an important concept that stems from the jellium model[83]. The total 16 electronic shell-closing ligand-protected gold clusters (all from previous experiments) are summarized in Supplementary Table 1. Cheng *et al.* developed the super valence bond (SVB) model[84] to explain the electronic stability of non-spherical shells of $Au_{38}(SR)_{24}$ (ref. 53). They suggest that the bi-icosahedral $Au_{23}^{(+9)}$ core of $Au_{38}(SR)_{24}$ can be viewed as a superatomic molecule. Later, the superatom network (SAN)[66] model, coupled with the adaptive natural density partitioning analysis[85], have been also invoked by Cheng *et al.* to explain the high stability of certain low-symmetry ligand-protected gold clusters. A key notion in the SAN model is that the core of Au nanoclusters can be viewed as a network of *n*-centered two-electron ($n = 2$–6) superatoms. A tetrahedral unit with two valence electrons has also been identified by Jin and co-workers[58] through an account of the number of valence electrons and tetrahedral units in a serial of structurally resolved double-helical gold clusters ($Au_{28}(SR)_{20}$, $Au_{36}(SR)_{24}$, $Au_{44}(SR)_{28}$ and $Au_{52}(SR)_{32}$)[44,49,56,58]. Recently, the Borromean-ring diagrams for the $Au_{25}(SR)_{18}$ (refs 42,43), $Au_{38}(SR)_{24}$ (ref. 53) and $Au_{102}(SR)_{44}$ (ref. 60) clusters have been proposed by Pradeep, Whetten and co-workers[86] to explain high stabilities of these clusters. All the theoretical models developed thus far are mainly to address stabilities of a subset of gold nanoclusters, rather than the entire set of 71 reported liganded gold clusters. As such, exceptional cases to these independent models abound. Hence, a grand unified model that can go beyond these previously developed models (SAC, SVB, SAN and so on) for understanding stabilities of all ligand-protected gold clusters is called for. Here we present a grand unified model (GUM) that can offer a universal description of the structures of diverse liganded gold clusters.

In this communication, the triangular elementary block $Au_3(2e)$ and tetrahedral elementary block $Au_4(2e)$ are identified to describe the stabilities of 71 liganded gold nanoclusters (Supplementary Table 2) reported up to date. On the basis of the GUM, deeper insights into structure evolution of the liganded gold nanoclusters can be obtained, namely, the structure evolution of the gold core cannot be viewed simply as addition of Au atoms, but rather as seamless packing of the elementary blocks. In addition, several stable liganded gold clusters are predicted.

Results

GUM development and quark model analogy. The development of the GUM is based on detailed analysis of the structures of all 71 liganded gold clusters (Supplementary Table 2) either determined from previous experiments (54 crystallized structures) or predicted from density-functional theory computation (17 structures) over the past three decades. The scheme of grand conceptual unification of the diverse structures of these 71 liganded gold clusters is motivated from the quark model in particle physics wherein six types of quarks, known as flavours, are conceptualized as a unification scheme for composite particles, such as protons and neutrons, and exotic hadrons, in terms of their valence quarks. For instance, it is known that protons, neutrons alike are not elementary but are viewed as bound states of the elementary valence quarks and antiquarks. All quarks are characterized by a set of quantum numbers, such as fractional electric charge of $\pm 2/3$ or $\pm 1/3$. In an analogous fashion, here, we assign a gold atom as the 'elementary particle' but with one of three 'flavours' due to its three possible valence states, that is, 1*e*, 0.5*e* and 0*e*. The three flavours are named as bottom, middle and top, respectively. Through close inspection of the 71 known clusters, we identify two 'composite particles', namely, the triangular Au_3 and tetrahedral Au_4 elementary blocks, in analogy to the protons and tetraquarks, respectively. We find that both elementary blocks satisfy the duet rule, that is, the high tendency of having two electrons in the valence shell. As a result, depending on the flavour of each constituent gold atom, the triangular elementary block can exhibit in total 10 variants of valence states (named as Δ_1–Δ_{10}), whereas the tetrahedral elementary block can exhibit in total 15 variants of valence states (named as T_1–T_{15}) (Fig. 1). We show that for all 71 liganded gold clusters, once the outer ligands are effectively detached from the inner Au cores (see below), the resulting Au cores are universally packed by the elementary blocks. Hence, the stabilities of the liganded gold clusters are due to the high stability of each individual elementary block.

Duet rule. Note that the duet rule elucidated here is akin to the textbook octet rule, a well-known and the first chemical rule of thumb in general chemistry. The octet rule is a valence-electron counting rule for the explanation or prediction of electronic structure and chemical bonding of molecules made of main-group elements. The other two valence-electron counting rules (that is, the second and third rules of thumb), namely, the 18-electron rule and Wade's rule, are newer chemical rules of thumb for understanding chemical structures of organometallics and polyhedral cluster compounds, respectively. Below, we report that in conjunction with the GUM, the duet rule of the valence shell for the elementary blocks can be treated as the fourth rule of thumb for understanding diverse liganded gold clusters.

Evidences on stabilities of the elementary blocks. In GUM, both elementary blocks triangular Au_3 and tetrahedral Au_4 entail only two valence electrons [$Au_3(2e)$ and $Au_4(2e)$], thereby both having strong electron shell closures. As shown in Fig. 2, the two valence electrons are delocalized in the shell-closing elementary blocks $Au_3(2e)$ and $Au_4(2e)$, consistent with the SAC model[82]. Moreover, from an experimental perspective, the Au_3 core of crystallized $[Au_3(IDipp)_3]^{1+}$ [IDipp = 1,3-bis(2,6-diisopropylphenyl)imidazol-2-ylidene] (ref. 5) and the Au_4 core of $[Au_4(PR_3)_4]^{2+}$ (ref. 6) (Supplementary Table 2) are essentially

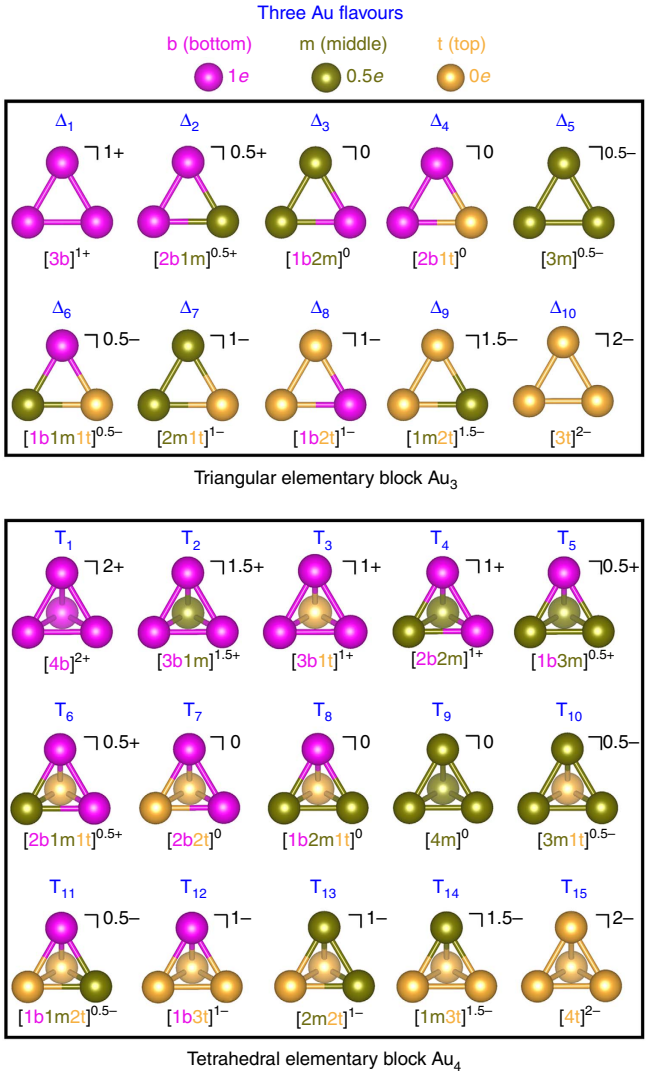

Figure 1 | Valence states of the triangular and tetrahedral elementary blocks. Ten variants (Δ_1-Δ_{10}) of valence states for the triangular elementary block Au_3 and 15 variants (T_1-T_{15}) of valence states for the tetrahedral elementary block Au_4 due to constituent Au atoms having three possible flavours (b for bottom flavour, m for middle flavour and t for top flavour), and the requirement of duet rule (that is, having 2e valence electrons). Colour code of Au atom: magenta (b), dark yellow (m) and yellow (t).

the same as the elementary blocks $Au_3(2e)$ and $Au_4(2e)$, respectively, supporting the high stabilities of the $Au_3(2e)$ and $Au_4(2e)$. The high stabilities of $Au_3(2e)$ and $Au_4(2e)$ structures can be also shown from *ab initio* computation. In Supplementary Table 3, the formation energies of five isoelectronic species, $Au_2(2e)$, $Au_3(2e)$, $Au_4(2e)$, $Au_5(2e)$ and $Au_6(2e)$, are listed. Only the triangular $Au_3(2e)$ and tetrahedral $Au_4(2e)$ exhibit highly negative formation energies, which provides another piece of strong evidence of their high stabilities. In addition, both elementary blocks exhibit larger highest/lowest occupied/unoccupied molecular orbital (HOMO/LUMO) gaps than their isoelectronic counterparts (Supplementary Table 3).

Electron counting protocols for effective detachment of ligands. All ligand-protected Au clusters are composed of an inner Au core and a number of outer ligands. The first step toward developing the GUM is to find effective protocols to

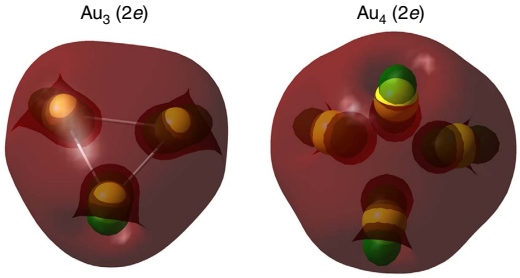

Figure 2 | The computed delocalized occupied orbitals ($1S^2$) of $Au_3(2e)$ (left) and $Au_4(2e)$ (right). Colour code: Au—yellow.

detach the protection ligands from the Au core so that the vast complex factors of the outer ligands can be removed while all ligand-protected Au clusters can be reduced to bare Au cores for structural analysis. Note that different elements or functional groups that are directly bonded with an Au atom at the core surface are in different valence-electron states. As such, if one is to focus on the valence state of the inner Au core, equivalent electron counting is required to effectively detach all protection ligands from the Au core. The following electron-counting protocols for effective detachment of different types of ligands can be undertaken (see Fig. 3 for graphical illustrations):

First, each SR group and Au atom embedded in the gold–thiolate staple motifs possess $-1e$ and $1e$ valence electron, respectively. To effectively detach the smallest staple motif from the Au core, the net number of valence electrons of the staple motif should be converted to zero. To this end, each of the two Au atoms (on the Au core) bonded with SR is considered to transfer $0.5e$ valence electron to the staple motif. As such, equivalent electron counting for effective detachment of the staple motif is achieved (Fig. 3a). Second, for SR group bonded with two Au atoms on the Au core, again, each of the two Au atoms (on the core) is considered to transfer $0.5e$ valence electron to the SR group so that equivalent electron counting for effective detachment of the SR group is achieved (Fig. 3b). Third, for halogen ligand X (X = F, Cl, Br and I) bonded with a single Au atom on the Au core, each Au atom is considered to transfer $1e$ valence electron to the X atom so that equivalent electron counting for effective detachment of the X atom is achieved (Fig. 3c). Fourth, the phosphine group is known as a weak ligand, thereby possessing $0e$ valence electron. As such, each Au atom bonded with the phosphine group still maintain its original $1e$ valence electron upon detachment with the phosphine group (Fig. 3d).

In summary, depending on the ligands, for example, PR_3, X, SR or gold–thiolate staple motifs, Au atoms on the Au core can exhibit one of the three flavours: bottom ($1e$), middle ($0.5e$) and top ($0e$) after effective detachment of the protection ligands from the Au core. Note also that when two elementary blocks are fused together via sharing a single Au atom, the shared Au atom contributes $0.5e$ valence electron to each elementary block. As such, the fused elementary blocks can be effectively separated via the protocol shown in Fig. 3e.

Prototypical liganded clusters. As shown in Supplementary Table 2, once the ligands are effectively detached from the Au cores, the Au cores of all 71 ligand-protected gold clusters can be universally decomposed into a number of the triangular Au_3 (Δ_1–Δ_{10}) and/or tetrahedral Au_4 (T_1–T_{15}) elementary blocks. Two prototypical structures are analysed here as two examples while other eight representative structures are either briefly

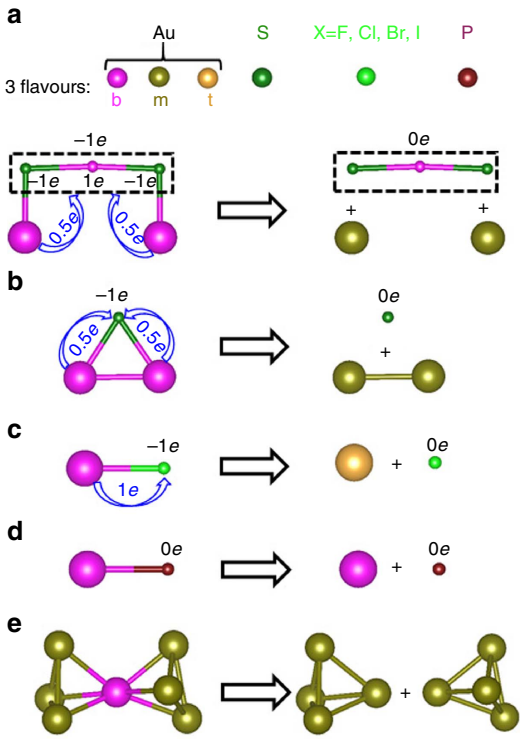

Figure 3 | Electron counting protocols for effective detachment of ligands from inner Au core. There are four cases for Au atom bonded with (**a**) gold-thiolate staple motifs, (**b**) SR, (**c**) X (X = F, Cl, Br and I) and (**d**) PR_3 functional groups; (**e**) effective separation of an Au atom shared by two elementary blocks. The blue arrow denotes charge transfer. Colour code: Au—magenta (bottom flavour), dark yellow (middle flavour) and yellow (top flavour); S—dark green; X—light green; P—wine. The R groups are omitted for clarity.

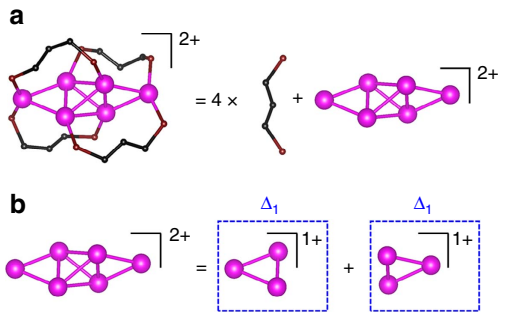

Figure 4 | The structural decomposition of $[Au_6(dppp)_4]^{2+}$. (**a**) The decomposition of $[Au_6(dppp)_4]^{2+}$ cluster into four ligands and an Au core. (**b**) The decomposition of the inner Au core into two triangular Au_3 elementary blocks, each block being in the Δ_1 valence state. Colour code: Au—magenta (bottom flavour); C—black; P—wine. The R groups are omitted for clarity.

illustrated here or elaborated in the Supplementary Figs 1–8. The remaining cases can be analysed in similar fashion.

The first prototype structure we consider is $[Au_6(dppp)_4]^{2+}$ (dppp = 1,3-Bis(diphenylphosphino)propane)[9], which is composed of four dppp ligands (each with 0*e* valence electron) and an Au_6^{2+} core (Fig. 4a). The Au_6 core consists of two triangular Au_3 blocks. According to the electron-counting protocol, the six Au atoms of the Au_6 core are all bonded with phosphine ligands and thus have 1*e* valence electron or the bottom flavour. Two positive charges are equally distributed in

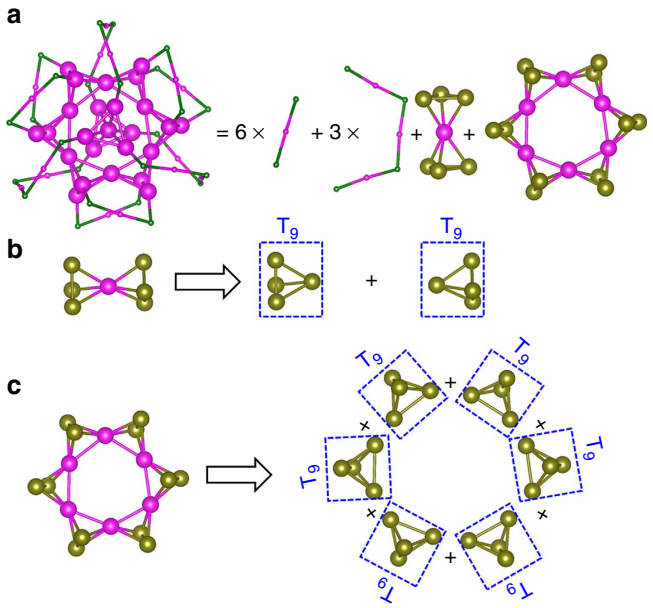

Figure 5 | The structural decomposition of $Au_{40}(SR)_{24}$. (**a**) The decomposition of $Au_{40}(SR)_{24}$ cluster into nine ligands and an Au core with two shells. (**b**) The decomposition of inner shell of the Au core into two fused tetrahedral Au_4 elementary blocks, each block, when separated, being in the T_9 valence state. (**c**) The decomposition of the outer shell of the Au core into six fused tetrahedral Au_4 elementary blocks in a loop, each block, when separated, being in the T_9 valence state. Colour code: Au—magenta (bottom flavour) and dark yellow (middle flavour); S—dark green. The R groups are omitted for clarity.

the two triangular Au_3 blocks. Thus, both triangular Au_3 elementary blocks are in the Δ_1 valence state (Fig. 4b).

The second prototype structure we consider is $Au_{40}(SR)_{24}$ (ref. 56). The Au core of $Au_{40}(SR)_{24}$ can be viewed as a combination of an Au_7 and a Kekulé-like Au_{18} structure (Fig. 5a). The Au_7 core is composed of two tetrahedral Au_4 blocks, fused together by sharing an Au atom. The latter contributes 0.5*e* valence electron to each tetrahedral Au_4 block. Other six vertex Au atoms are bonded with the SR group and each contributes 0.5*e* valence electron to the resident tetrahedral Au_4 block. Thus, each of the four vertex Au atoms in the tetrahedral Au_4 block has the middle flavour so that each tetrahedral Au_4 elementary block is in the T_9 valence state (Fig. 5b). Moreover, the Kekulé-like Au_{18} structure can be viewed as six tetrahedral Au_4 blocks fused together in a loop with six sharing Au atoms (Fig. 5c). Again, each of the six tetrahedral Au_4 elementary blocks is in the T_9 valence state.

Finally, eight other representative clusters are considered. The structure decompositions of eight other representative clusters in terms of elementary blocks as well as their corresponding valence states are shown in Supplementary Figs 1–8. Specifically, the structure decomposition of three largest ligand-protected gold clusters, $Au_{102}(SR)_{44}$ (ref. 60), $Au_{130}(SR)_{50}$ (ref. 61) and $Au_{144}(SR)_{60}$ (ref. 78), are given below. According to the 'divide-and-protect' formulation[87,88], the $Au_{102}(SR)_{44}$ can be written as $Au_{79}[RS\text{-}Au\text{-}SR]_{19}[RS\text{-}Au\text{-}SR\text{-}Au\text{-}SR]_2$. Each of the two Au atoms in the $Au_{102}(SR)_{44}$ shared by two [-RS-Au-SR-] staple motifs can be viewed as the Au atom with 0*e* valence electron (that is, top flavour). As such, the Au_{79} core of $Au_{102}(SR)_{44}$ is composed of 29 elementary blocks and their corresponding valence states can be described by [$5\Delta_1$, Δ_3, $16\Delta_5$, $2T_4$, $2T_5$, T_7 and $2T_9$] (Supplementary Fig. 9), giving rise to 58 valence electrons in total (corresponding to the strong electron

shell closure, according to SAC model[82]) for $Au_{102}(SR)_{44}$. The Au_{105} core of $Au_{130}(SR)_{50}$ is composed of 40 elementary blocks and their corresponding valence states include $5\Delta_3$, $11\Delta_5$, $4T_4$, $3T_5$ and $17T_9$ (Supplementary Fig. 10), giving rise to 80 valence electrons in total for $Au_{130}(SR)_{50}$. The Au_{114} core of $Au_{144}(SR)_{60}$ is composed of 42 elementary blocks and their corresponding valence states include $20\Delta_5$, $13T_4$, $3T_5$ and $6T_9$ (Supplementary Fig. 11), giving rise to 84 valence electrons in total in $Au_{144}(SR)_{60}$.

Discussion

In general, the inner Au cores of all the ligand-protected gold clusters are composed of elementary blocks (Supplementary Table 2 and Fig. 6), each having two valence electrons (Fig. 1), whereas the outer ligands with 0*e* valence electron provide the geometry constraint and arrangement of valence electrons in each elementary block to satisfy the duet rule. In Supplementary Fig. 12, we show several possible valence states for two fused tetrahedral Au_4 blocks (Au_7) protected by either SR or PR_3 groups in various liganded gold clusters. Our analysis indicates that the fused tetrahedral Au_4 elementary blocks in the four predicted stable clusters, $Au_{10}(SR)_6$, $[Au_9(SR)_4(PR_3)_2]^{1+}$, $[Au_8(SR)_2(PR_3)_4]^{2+}$ and $[Au_7(PR_3)_6]^{3+}$, are in the $2T_9$, $2T_5$, $2T_4$ and $2T_2$ valence states, respectively, whereas the constructed $Au_8(SR)_2(PR_3)_4$ and $Au_7(PR_3)_6$ clusters are expected to be less stable due to their violation of the duet rule. Note that a recent experimental investigation of $Au_{25}(SR)_{18}$ in its three oxidation states, that is, $Au_{25}(SR)_{18}^{-1/0/+1}$, provides more compiling evidence on the effect of violation of the duet rule (or deviation from the strong electron shell closure) to the symmetry of the Au_{13} core and stability of the cluster[89]. The obtained three crystalline structures in the related three oxidation states demonstrate that the structural distortion (in the Au core in particular) increases with the decreased superatomic valence from $1S^21P^6$ to $1S^21P^4$ as the $Au_{25}(SR)_{18}^{-1}$ cluster has the eight-electron shell-closing configuration[82] $1S^21P^6$, and thus the highest thermal stability. The other two oxidation states, $Au_{25}(SR)_{18}^{0/+1}$, are less stable due to the incomplete 1P superatomic orbital. Likewise, the structural distortion observed in the two oxidation states, $Au_{25}(SR)_{18}^{0/+1}$, can be understood based on GUM. The Au_{13} core of $Au_{25}(SR)_{18}^{-1}$ can be decomposed into four elementary blocks and their corresponding valence states can be described as [$2\Delta_5$ and $2T_9$] (Supplementary Table 2). Clearly, the number of valence electrons in both oxidation states, $Au_{25}(SR)_{18}^{0/+1}$, dissatisfies the duet rule. As a consequence, lower thermal stability and larger structural distortion in the highly symmetric Au_{13} core are expected, consistent with the experimental evidence[89].

The GUM does not only offer a universal structural characterization of all 71 liganded gold clusters, but it also provides deeper insights into structure evolution of the Au clusters. In Fig. 6, a structure evolution map for the Au cores with increasing number of elementary blocks is presented. Indeed, the structure evolution of the Au cores can be understood through various routes of packing the elementary blocks. For example, two elementary blocks with T_9 valence state can yield either the Au_8 core of $Au_{24}(SR)_{20}$ (ref. 39) via direct packing or the Au_7 core of $Au_{20}(SR)_{16}$ (ref. 33) via sharing a vertex Au atom. Two elementary blocks with T_4 valence states can give rise to the

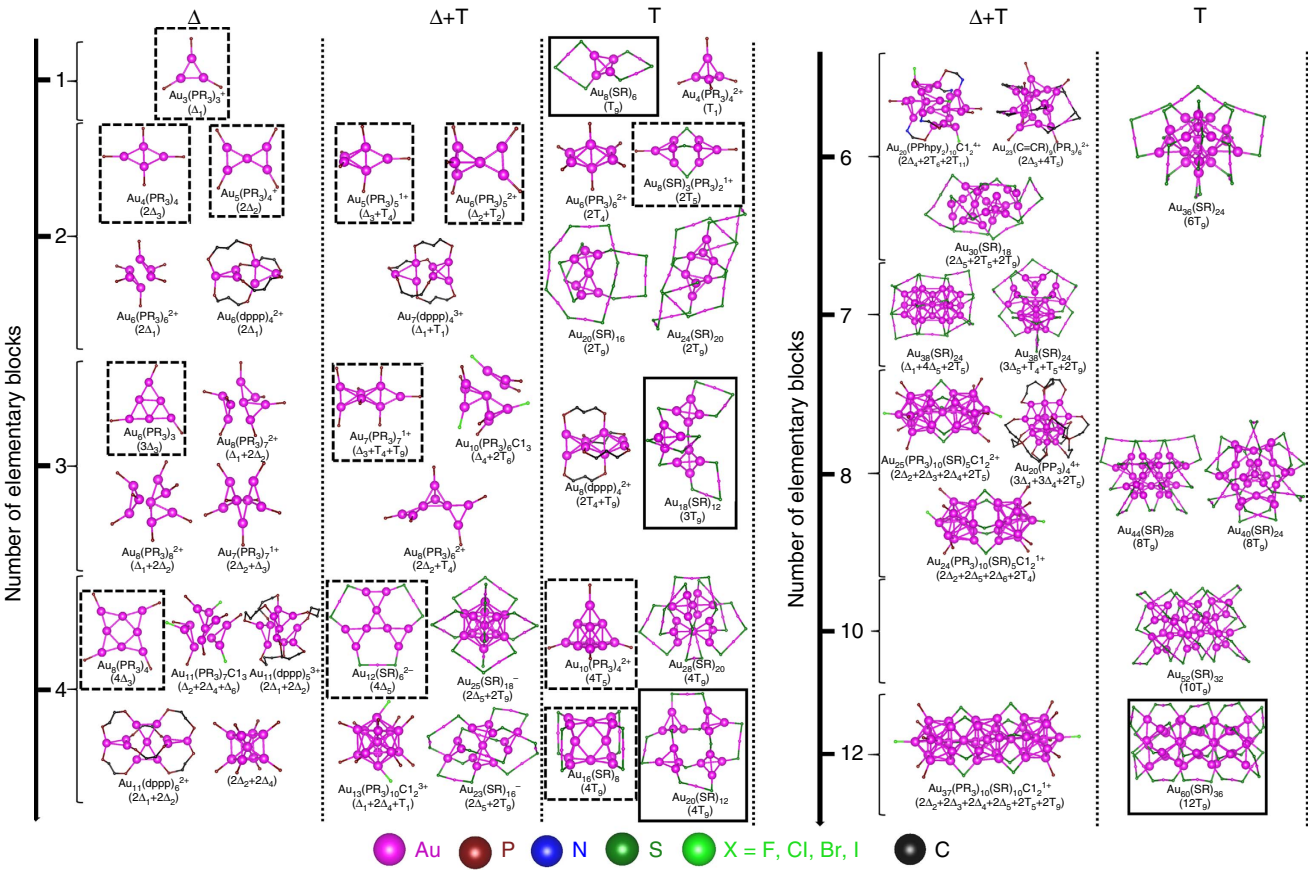

Figure 6 | Structure evolution of the Au cores (large magenta spheres) with increasing number of elementary blocks. Colour code: Au—magenta; S—dark green; X—light green; P—wine; C—black; N—blue. The R groups are omitted for clarity. The dotted and solid squares denote the newly and previously predicted structures, respectively. Others are crystallized structures.

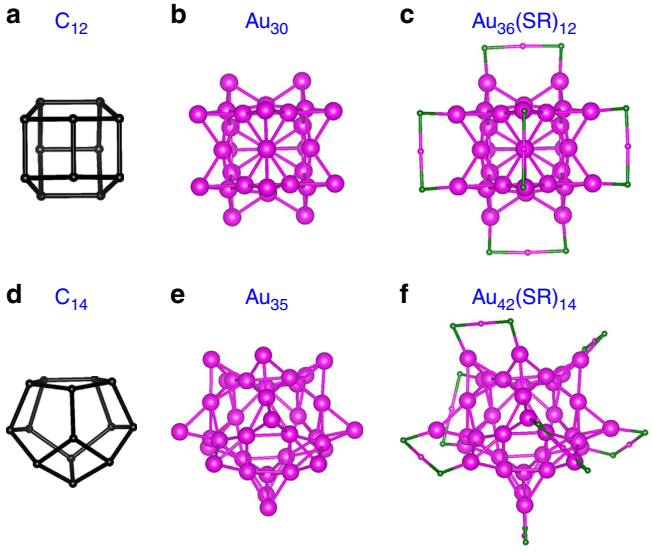

Figure 7 | Two predicted $Au_{36}(SR)_{12}$ and $Au_{42}(SR)_{14}$ clusters based on GUM using C_{12} and C_{14} fullerenes as templates. Structures of a C_{12} fullerene (**a**), Au_{30} core (**b**) and $Au_{36}(SR)_{12}$ cluster (**c**), as well as C_{14} fullerene (**d**), Au_{35} core (**e**) and $Au_{42}(SR)_{14}$ cluster (**f**). Colour code: Au—magenta; S—dark green; C—black. The R groups are omitted for clarity.

Au_6 core of $[Au_6(PR_3)_6]^{2+}$ (ref. 7) through sharing one common edge. With gradually increasing the number of elementary blocks, larger Au core structures can be formed while adjusting the overall charge of the liganded gold clusters to meet the duet rule. In summary, the structure evolution of the Au core cannot be viewed simply as addition of Au atoms (Supplementary Fig. 13), but rather as seamless packing of the elementary blocks while obeying the duet rule.

In addition to structure unification, the GUM can be utilized for predicting new structures of liganded gold clusters. From the structure evolution map shown in Fig. 6, one can see that there are many vacant spaces, suggesting many missing liganded gold clusters yet to be synthesized. We construct a series of ligand-protected gold clusters (shown in dotted squares in Fig. 6) on the basis of GUM to fill some vacant spaces in Fig. 6. The elementary blocks and their valence states for the Au cores of all constructed clusters are depicted in Supplementary Fig. 14. These clusters exhibit large computed HOMO–LUMO gaps (Supplementary Table 4), suggesting potentially high chemical stabilities.

In particular, a class of hitherto unreported ligand-protected hollow Au clusters are presented here. For example, $Au_{36}(SR)_{12}$ can be constructed by using the C_{12} fullerene as a template. C_{12} fullerene exhibits eight polygons: four quadrilaterals and four pentagons (Fig. 7a). Replacing all C atoms of the C_{12} fullerene with 12 fused tetrahedral Au_4 gives rise to the Au_{30} core (Fig. 7b) of $Au_{36}(SR)_{12}$, followed by adding [-RS-Au-SR-] staple motifs on the unfused Au atoms to build the complete $Au_{36}(SR)_{12}$ cluster (Fig. 7c). The Au_{30} hollow cage in $Au_{36}(SR)_{12}$ is composed of 12 fused elementary blocks all at the T_9 valence state. The $Au_{36}(SR)_{12}$ cluster exhibits a large computed HOMO–LUMO gap of 2.20 eV and has no imaginary vibrational frequencies. An *ab initio* molecular dynamics simulation of the $Au_{36}(SR)_{12}$ cluster at 355 K for 10 ps suggests high thermal stability of the $Au_{36}(SR)_{12}$ cluster (Supplementary Fig. 15 and Supplementary Methods). Figure 7f shows another example of ligand-protected hollow Au cluster, namely, $Au_{42}(SR)_{14}$, constructed by using the C_{14} fullerene (Fig. 7d) as a template. The Au_{35} hollow cage (Fig. 7e) in $Au_{42}(SR)_{14}$ is composed of 14 fused elementary blocks all at the T_9 valence state. The computed HOMO–LUMO gap of $Au_{42}(SR)_{14}$ is 2.00 eV, suggesting high chemical stability. Interestingly, the $Au_{36}(SR)_{12}$ and $Au_{42}(SR)_{14}$ can be rewritten as $Au_{30}[Au(SR)_2]_6$ and $Au_{35}[Au(SR)_2]_7$, respectively, consistent with the 'divide-and-protect' formulation[87,88].

In conclusion, a grand unified model that can incorporate previously developed independent models (SAC, SVB, SAN and so on.) is developed to address stabilities of all ligand-protected gold clusters. On the basis of the GUM, all 71 liganded gold nanoclusters can be decomposed into several elementary blocks of triangular $Au_3(2e)$ and tetrahedral $Au_4(2e)$. Although GUM is a predictive heuristic and may not be necessarily reflective of the actual electronic structure, a series of highly stable liganded gold clusters are predicted, which provides a guide to synthesizing new ligand-protected gold clusters. Hence, the GUM can offer not only new insights into the packing and structure evolution of the 71 liganded gold clusters known as of today, but also a systematic route toward rational design and characterization of liganded metal clusters to inspire future experimental synthesis.

Data availability. The authors declare that the data supporting the findings of this study are available within the article and its Supplementary Information files, and all relevant data are available from the authors.

References

1. Turner, M. *et al.* Selective oxidation with dioxygen by gold nanoparticle catalysts derived from 55-atom clusters. *Nature* **454,** 981–984 (2008).
2. Chen, S. *et al.* Gold nanoelectrodes of varied size: transition to molecule-like charging. *Science* **280,** 2098–2101 (1998).
3. Daniel, M. C. & Astruc, D. Gold nanoparticles: assembly, supramolecular chemistry, quantum-size-related properties, and applications toward biology, catalysis, and nanotechnology. *Chem. Rev.* **104,** 293–346 (2004).
4. Rosi, N. L. *et al.* Oligonucleotide-modified gold nanoparticles for intracellular gene regulation. *Science* **312,** 1027–1030 (2006).
5. Robilotto, T. J., Bacsa, J., Gray, T. G. & Sadighi, J. P. Synthesis of a trigold monocation: an isolobal analogue of $[H_3]^+$. *Angew. Chem.* **124,** 12243–12246 (2012).
6. Zeller, E., Beruda, H. & Schmidbaur, H. Tetrahedral gold cluster $[Au_4]^{2+}$: crystal structure of $\{[(^tBu)_3PAu]_4\}^{2+}(BF_4^-)_2\cdot 2CHCl_3$. *Inorg. Chem.* **32,** 3203–3204 (1993).
7. Briant, C. E., Hall, K. P., Mingos, D. M. P. & Wheeler, A. C. Synthesis and structural characterisation of hexakis (triphenyl phosphine)-hexagold (2+) nitrate, $[Au_6(PPh_3)_6][NO_3]_2$, and related clusters with edge-sharing bitetrahedral geometries. *J. Chem. Soc. Dalton Trans.* 687–692 (1986).
8. Bellon, P., Manassero, M. & Sansoni, M. An octahedral gold cluster: crystal and molecular structure of hexakis[tris-(p-tolyl)phosphine]-octahedro-hexagold bis(tetraphenylborate). *J. Chem. Soc. Dalton Trans.* 2423–2427 (1973).
9. Van Der Velden, J. W. A. *et al.* Gold clusters. Tetrakis[1,3-bis(diphenylphosphino)propane]hexagold dinitrate: preparation, x-ray analysis, and gold-197 Moessbauer and phosphorus-31{proton} NMR spectra. *Inorg. Chem.* **21,** 4321–4324 (1982).
10. Van Der Velden, J. W. A. *et al.* Intermediates in the formation of gold clusters. Preparation and x-ray analysis of $[Au_7(PPh_3)_7]^+$ and synthesis and characterization of $[Au_8(PPh_3)_6I]PF_6$. *Inorg. Chem.* **23,** 146–151 (1984).
11. Shichibu, Y., Zhang, M., Kamei, Y. & Konishi, K. $[Au_7]^{3+}$: a missing link in the four-electron gold cluster family. *J. Am. Chem. Soc.* **136,** 12892–12895 (2014).
12. Kobayashi, N., Kamei, Y., Shichibu, Y. & Konishi, K. Protonation-induced chromism of pyridylethynyl-appended [core + exo]-type Au_8 clusters. Resonance-coupled electronic perturbation through π-conjugated group. *J. Am. Chem. Soc.* **135,** 16078–16081 (2013).
13. Kamei, Y., Shichibu, Y. & Konishi, K. Generation of small gold clusters with unique geometries through cluster-to-cluster transformations: Octanuclear clusters with edgesharing gold tetrahedron motifs. *Angew. Chem. Int. Ed.* **50,** 7442–7445 (2011).
14. Manassero, M., Naldini, L. & Sansoni, M. A new class of gold cluster compounds. Synthesis and *X*-ray structure of the octakis(triphenylphosphinegold) dializarinsulphonate, $[Au_8(PPh_3)_8](aliz)_2$. *J. Chem. Soc., Chem. Commun.* 385–386 (1979).
15. Van Der Velden, J. W. A., Bour, J. J., Bosman, W. P. & Noordik, J. H. Synthesis and *X*-ray crystal structure determination of the cationic gold cluster

compound $[Au_8(PPh_3)_7](NO_3)_2$. *J. Chem. Soc., Chem. Commun.* 1218–1219 (1981).
16. Yang, Y. & Sharp, P. R. New gold clusters $[Au_8L_6](BF_4)_2$ and $[(AuL)_4](BF_4)_2$ (L = P(mesityl)$_3$. *J. Am. Chem. Soc.* **116,** 6983–6984 (1994).
17. Bellon, P. L., Cariati, F., Manassero, M., Naldini, L. & Sansoni, M. Novel gold clusters. Preparation, properties, and X-ray structure determination of salts of octakis(triarylphosphine)enneagold, $[Au_9L_8]X_3$. *J. Chem. Soc. D* 1423–1424 (1971).
18. Cooper, M. K., Dennis, G. R., Henrick, K. & Mcpartlin, M. A new type of gold cluster compound. The syntheses and X-ray structure analysis of pentakis (tricyclohexylphosphino) tris (thiocyanato) enneagold, $[Au_9\{P(C_6H_{11})_3\}_5(SCN)_3]$, and bis {tri (cyclohexyl) phosphinato} gold (I) hexafluorophosphate, $[Au\{P(C_6H_{11})_3\}_2][PF_6]$. *Inorg. Chim. Acta.* **45,** L151–L152 (1980).
19. Van Der Velden, J. W. A., Bour, J. J., Bosman, W. P., Noordik, J. H. & Beurskens, P. T. The electrochemical preparation of $[Au_9(PPh_3)_8]^+$. A comparative study of the structures and properties of $[Au_9(PPh_3)_8]^+$ and $[Au_9(PPh_3)_8]^{3+}$. *Recl. Trav. Chim. Pays-Bas* **103,** 13–16 (1984).
20. Briant, C. E., Hall, K. P., Wheeler, A. C. & Mingos, D. M. P. Structural characterisation of $[Au_{10}Cl_3(PCy_2Ph)_6](NO_3)$(Cy = cyclohexyl) and the development of a structural principle for high nuclearity gold clusters. *J. Chem. Soc.,Chem. Commun.* 248–250 (1984).
21. Nunokawa, K. *et al.* Synthesis, single crystal X-ray analysis, and TEM for a single-sized Au_{11} cluster stabilized by SR ligands: The interface between molecules and particles. *J. Organomet. Chem.* **691,** 638–642 (2006).
22. Shichibu, Y., Kamei, Y. & Konishi, K. Unique [core + two] structure and optical property of a dodeca-ligated undecagold cluster: critical contribution of the exo gold atoms to the electronic structure. *Chem. Commun.* **48,** 7559–7561 (2012).
23. Smits, J. M. M., Bour, J. J., Vollenbroek, F. A. & Beurskens, P. T. Preparation and X-ray structure determination of [pentakis{1,3-bis(diphenylphosphino)propane}] undecagoldtris(thiocyanate), $[Au_{11}\{PPh_2C_3H_6PPh_2\}_5](SCN)_3$. *J. Cryst. Spectrosc.* **13,** 355–363 (1983).
24. Bellon, P., Manassero, M. & Sansoni, M. Crystal and molecular structure of tri-iodoheptakis(tri-*p*-fluorophenylphosphine)undecagold. *J. Chem. Soc. Dalton Trans.* 1481–1487 (1972).
25. McKenzie, L. C., Zaikova, T. O. & Hutchison, J. E. Structurally similar triphenylphosphine-stabilized undecagolds, $Au_{11}(PPh_3)_7Cl_3$ and $[Au_{11}(PPh_3)_8Cl_2]Cl$, exhibit distinct ligand exchange pathways with glutathione. *J. Am. Chem. Soc.* **136,** 13426–13435 (2014).
26. Briant, C. E., Tobald, B. R. C., White, J. W., Bell, L. K. & Mingos, D. M. P. Synthesis and X-ray structural characterization of the centered icosahedral gold cluster compound $[Au_{13}(PMe_2Ph)_{10}Cl_2](PF_6)_3$; the realization of a theoretical prediction. *J. Chem. Soc. Chem. Commun.* **5,** 201–202 (1981).
27. Gutrath, B. S. *et al.* $[Au_{14}(PPh_3)_8(NO_3)_4]$: an example of a new class of Au(NO_3)-ligated superatom complexes. *Angew. Chem. Int. Ed.* **52,** 3529–3532 (2013).
28. Das, A. *et al.* Structure determination of $[Au_{18}(SR)_{14}]$. *Angew. Chem. Int. Ed.* **54,** 3140–3144 (2015).
29. Chen, S. *et al.* The structure and optical properties of the $[Au_{18}(SR)_{14}]$ nanocluster. *Angew. Chem. Int. Ed.* **54,** 3145–3149 (2015).
30. Wan, X., Tang, Q., Yuan, S., Jiang, D. & Wang, Q. M. Au_{19} nanocluster featuring a V − shaped alkynyl − gold motif. *J. Am. Chem. Soc.* **137,** 652–655 (2015).
31. Wan, X., Tang, Q., Yuan, S., Jiang, D. & Wang, Q. M. Au_{20} nanocluster protected by hemilabile phosphines. *J. Am. Chem. Soc.* **134,** 14750–14752 (2012).
32. Wan, X., Yuan, S., Lin, Z. & Wang, Q. M. A chiral gold nanocluster Au_{20} protected by tetradentate phosphine ligands. *Angew. Chem. Int. Ed.* **53,** 2923–2926 (2014).
33. Zeng, C., Liu, C., Chen, Y., Rosi, N. L. & Jin, R. Gold-thiolate ring as a protecting motif in the $Au_{20}(SR)_{16}$ nanocluster and implications. *J. Am. Chem. Soc.* **136,** 11922–11925 (2014).
34. Chen, S. *et al.* Total structure determination of Au_{21}(S-Adm)$_{15}$ and geometrical/electronic structure evolution of thiolated gold nanoclusters. *J. Am. Chem. Soc.* **138,** 10754–10757 (2016).
35. Wan, X., Yuan, S., Tang, Q., Jiang, D. & Wang, Q. M. Alkynyl-protected Au_{23} nanocluster: a 12-electron system. *Angew. Chem. Int. Ed.* **54,** 5977–5980 (2015).
36. Das, A. *et al.* Nonsuperatomic $[Au_{23}(SC_6H_{11})_{16}]^-$ nanocluster featuring bipyramidal Au_{15} kernel and trimeric $Au_3(SR)_4$ motif. *J. Am. Chem. Soc.* **135,** 18264–18267 (2013).
37. Wan, X. *et al.* A near-infrared-emissive alkynyl-protected Au_{24} nanocluster. *Angew. Chem. Int. Ed.* **54,** 9683–9686 (2015).
38. Crasto, D. *et al.* $Au_{24}(Sadm)_{16}$ nanomolecules: X-ray crystal structure, theoretical analysis, adaptability of adamantane ligands to form $Au_{23}(Sadm)_{16}$ and $Au_{25}(Sadm)_{16}$, and its relation to $Au_{25}(SR)_{18}$. *J. Am. Chem. Soc.* **136,** 14933–14940 (2014).
39. Das, A. *et al.* Crystal structure and electronic properties of a thiolate-protected Au_{24} nanocluster. *Nanoscale* **6,** 6458–6462 (2014).
40. Das, A. *et al.* Total structure and optical properties of a phosphine/thiolate-protected Au_{24} nanocluster. *J. Am. Chem. Soc.* **134,** 20286–20289 (2012).
41. Shichibu, Y. *et al.* Biicosahedral gold clusters $[Au_{25}(PPh_3)_{10}(SC_nH_{2n+1})_5Cl_2]^{2+}$ (n = 2–18): a stepping stone to cluster-assembled materials. *J. Phys. Chem. C* **111,** 7845–7847 (2007).
42. Zhu, M., Aikens, C. M., Hollander, F. J., Schatz, G. C. & Jin, R. Correlating the crystal structure of a thiol-protected Au_{25} cluster and optical properties. *J. Am. Chem. Soc.* **130,** 5883–5885 (2008).
43. Heaven, M. W., Dass, A., White, P. S., Holt, K. M. & Murray, R. W. Crystal structure of the gold nanoparticle $[N(C_8H_{17})_4][Au_{25}(SCH_2CH_2Ph)_{18}]$. *J. Am. Chem. Soc.* **130,** 3754–3755 (2008).
44. Zeng, C., Li, T., Das, A., Rosi, N. L. & Jin, R. Chiral structure of thiolate-protected 28-gold-atom nanocluster determined by X-ray crystallography. *J. Am. Chem. Soc.* **135,** 10011–10013 (2013).
45. Chen, Y. *et al.* Isomerism in $Au_{28}(SR)_{20}$ nanocluster and stable structures. *J. Am. Chem. Soc.* **138,** 1482–1485 (2016).
46. Dass, A. *et al.* Crystal structure and theoretical analysis of green gold Au_{30}(S-tBu)$_{18}$ nanomolecules and their relation to Au_{30}S(S-tBu)$_{18}$. *J. Phys. Chem. C* **120,** 6256–6261 (2016).
47. Higaki, T. *et al.* Controlling the atomic structure of Au_{30} nanoclusters by a ligand-based strategy. *Angew. Chem. Int. Ed.* **55,** 6694–6697 (2016).
48. Crasto, D., Malola, S., Brosofsky, G., Dass, A. & Häkkinen, H. Single crystal XRD structure and theoretical analysis of the chiral Au_{30}S(S-t-Bu)$_{18}$ cluster. *J. Am. Chem. Soc.* **136,** 5000–5005 (2014).
49. Zeng, C. *et al.* Total structure and electronic properties of the gold nanocrystal $Au_{36}(SR)_{24}$. *Angew. Chem. Int. Ed.* **51,** 13114–13118 (2012).
50. Yang, S. *et al.* A new crystal structure of Au_{36} with a Au_{14} kernel cocapped by thiolate and chloride. *J. Am. Chem. Soc.* **137,** 10033–10035 (2015).
51. Jin, R. *et al.* Tri-icosahedral gold nanocluster $[Au_{37}(PPh_3)_{10}(SC_2H_4Ph)_{10}X_2]^+$: linear assembly of icosahedral building blocks. *ACS Nano* **9,** 8530–8536 (2015).
52. Liu, C. *et al.* Observation of body-centered cubic gold nanocluster. *Angew. Chem. Int. Ed.* **54,** 9826–9829 (2015).
53. Qian, H., Eckenhoff, W. T., Zhu, Y., Pintauer, T. & Jin, R. Total structure determination of thiolate-protected Au_{38} nanoparticles. *J. Am. Chem. Soc.* **132,** 8280–8281 (2010).
54. Tian, S. *et al.* Structural isomerism in gold nanoparticles revealed by X-ray crystallography. *Nat. Commun.* **6,** 8667 (2015).
55. Teo, B. K., Shi, X. & Zhang, H. Pure gold cluster of 1:9:9:1:9:9:1 layered structure: a novel 39-metal-atom cluster $[(Ph_3P)_{14}Au_{39}Cl_6]Cl_2$ with an interstitial gold atom in a hexagonal antiprismatic cage. *J. Am. Chem. Soc.* **114,** 2743–2745 (1992).
56. Zeng, C. *et al.* Gold tetrahedra coil up: Kekulé-like and double helical superstructures. *Sci. Adv.* **1,** e1500425 (2015).
57. Liao, L. *et al.* Structure of chiral Au_{44}(2,4-DMBT)$_{26}$ nanocluster with an 18-electron shell closure. *J. Am. Chem. Soc.* **138,** 10425–10428 (2016).
58. Zeng, C. *et al.* Gold quantum boxes: on the periodicities and the quantum confinement in the Au_{28}, Au_{36}, Au_{44}, and Au_{52} magic series. *J. Am. Chem. Soc.* **138,** 3950–3953 (2016).
59. Zeng, C., Liu, C., Chen, Y., Rosi, N. L. & Jin, R. atomic structure of self-assembled monolayer of thiolates on a tetragonal Au_{92} nanocrystal. *J. Am. Chem. Soc.* **138,** 8710–8713 (2016).
60. Jadzinsky, P. D., Calero, G., Ackerson, C. J., Bushnell, D. A. & Kornberg, R. D. Structure of a thiol monolayer-protected gold nanoparticle at 1.1 Å resolution. *Science* **318,** 430–433 (2007).
61. Chen, Y. *et al.* Crystal structure of barrel-shaped chiral Au_{130}(p-MBT)$_{50}$ nanocluster. *J. Am. Chem. Soc.* **137,** 10076–10079 (2015).
62. Dass, A. *et al.* Au_{133}(SPh-tBu)$_{52}$ nanomolecules: X-ray crystallography, optical, electrochemical, and theoretical analysis. *J. Am. Chem. Soc.* **137,** 4610–4613 (2015).
63. Zeng, C. *et al.* Structural patterns at all scales in a nonmetallic chiral $Au_{133}(SR)_{52}$ nanoparticle. *Sci. Adv.* **1,** e1500045 (2015).
64. Liu, C., Pei, Y., Sun, H. & Ma, J. The nucleation and growth mechanism of thiolate-protected Au nanoclusters. *J. Am. Chem. Soc.* **137,** 15809–15816 (2015).
65. Jiang, D., Overbury, S. H. & Dai, S. Structure of $Au_{15}(SR)_{13}$ and its implication for the origin of the nucleus in thiolated gold nanoclusters. *J. Am. Chem. Soc.* **135,** 8786–8789 (2013).
66. Cheng, L., Yuan, Y., Zhang, X. & Yang, J. Superatom networks in thiolate-protected gold nanoparticles. *Angew. Chem. Int. Ed.* **52,** 9035–9039 (2013).
67. Pei, Y., Gao, Y., Shao, N. & Zeng, X. C. Thiolate-protected $Au_{20}(SR)_{16}$ cluster: prolate Au_8 core with new $[Au_3(SR)_4]$ staple motif. *J. Am. Chem. Soc.* **131,** 13619–13621 (2009).

68. Pei, Y., Tang, J., Tang, X., Huang, Y. & Zeng, X. C. New structure model of $Au_{22}(SR)_{18}$: bitetrahederon golden kernel enclosed by $[Au_6(SR)_6]$ Au(I) complex. *J. Phys. Chem. Lett.* **6,** 1390–1395 (2015).
69. Pei, Y. *et al.* Interlocked catenane-like structure predicted in $Au_{24}(SR)_{20}$: implication to structural evolution of thiolated gold clusters from homoleptic gold(i) thiolates to core-stacked nanoparticles. *J. Am. Chem. Soc.* **134,** 3015–3024 (2012).
70. Akola, J., Walter, M., Whetten, R. L., Häkkinen, H. & Grönbeck, H. On the structure of thiolate-protected Au_{25}. *J. Am. Chem. Soc.* **130,** 3756–3757 (2008).
71. Tian, Z. & Cheng, L. Electronic and geometric structures of Au_{30} clusters: a network of 2e-superatom Au cores protected by tridentate protecting motifs with u_3-S. *Nanoscale* **8,** 826–834 (2016).
72. Pei, Y., Gao, Y. & Zeng, X. C. Structural prediction of thiolate-protected Au_{38}: a face-fused bi-icosahedral Au core. *J. Am. Chem. Soc.* **130,** 7830–7832 (2008).
73. Malola, S. *et al.* $Au_{40}(SR)_{24}$ cluster as a chiral dimer of 8-electron superatoms: Structure and optical properties. *J. Am. Chem. Soc.* **134,** 19560–19563 (2012).
74. Pei, Y., Lin, S. S., Su, J. & Liu, C. Structure prediction of $Au_{44}(SR)_{28}$: a chiral superatom cluster. *J. Am. Chem. Soc.* **135,** 19060–19063 (2013).
75. Xu, W. W., Gao, Y. & Zeng, X. C. Unraveling structures of protection ligands on gold nanoparticle $Au_{68}(SH)_{32}$. *Sci. Adv.* **1,** e1400211 (2015).
76. Xu, W. W., Li, Y., Gao, Y. & Zeng, X. C. Unraveling a generic growth pattern in structure evolution of thiolate-protected gold nanoclusters. *Nanoscale* **8,** 7396–7401 (2016).
77. Xu, W. W. & Gao, Y. Unraveling the atomic structures of the $Au_{68}(SR)_{34}$ nanoparticles. *J. Phys. Chem. C* **119,** 14224–14229 (2015).
78. Lopez-Acevedo, O., Akola, J., Whetten, R. L., Grönbeck, H. & Häkkinen, H. Structure and bonding in the ubiquitous icosahedral metallic gold cluster $Au_{144}(SR)_{60}$. *J. Phys. Chem. C* **113,** 5035–5038 (2009).
79. Wade, K. The structural significance of the number of skeletal bonding electron-pairs in carboranes, the higher boranes and borane anions, and various transition-metal carbonyl cluster compounds. *J. Chem. Soc. D* 792–793 (1971).
80. Mingos, D. M. P. A general theory for cluster and ring compounds of the main group and transition elements. *Nat. Phys. Sci.* **236,** 99–102 (1972).
81. Mingos, D. M. P. Molecular-orbital calculations on cluster compounds of gold. *J. Chem. Soc. Dalton Trans.* 1163–1169 (1976).
82. Walter, M. *et al.* A unified view of ligand-protected gold clusters as superatom complexes. *Proc. Natl Acad. Sci.* **105,** 9157–9162 (2008).
83. Ekardt, W. Dynamical polarizability of small metal particles: self-consistent spherical jellium background model. *Phys. Rev. Lett.* **52,** 1925–1928 (1984).
84. Cheng, L., Ren, C., Zhang, X. & Yang, J. New insight into the electronic shell of $Au_{38}(SR)_{24}$: a superatomic molecule. *Nanoscale* **5,** 1475–1478 (2013).
85. Zubarev, D. Y. & Boldyrev, A. I. Developing paradigms of chemical bonding: adaptive natural density partitioning. *Phys. Chem. Chem. Phys.* **10,** 5207–5217 (2008).
86. Natarajan, G., Mathew, A., Negishi, Y., Whetten, R. L. & Pradeep, T. A unified framework for understanding the structure and modifications of atomically precise monolayer protected gold clusters. *J. Phys. Chem. C* **119,** 27768–27785 (2015).
87. Pei, Y. & Zeng, X. C. Investigating the structural evolution of thiolate protected gold clusters from first-principles. *Nanoscale* **4,** 4054–4072 (2012).
88. Häkkinen, H., Walter, M. & Gronbeck, H. Divide and protect: capping gold nanoclusters with molecular gold-thiolate rings. *J. Phys. Chem. B* **110,** 9927–9931 (2006).
89. Tofanelli, M. A. *et al.* Jahn–Teller effects in $Au_{25}(SR)_{18}$. *Chem. Sci.* **7,** 1882–1890 (2016).

Acknowledgements

W.W.X. is supported by National Natural Science Foundation of China (11504396). Y.G. is supported by the start-up funding from Shanghai Institute of Applied Physics, Chinese Academy of Sciences (Y290011011), National Natural Science Foundation of China (21273268, 11574340), 'Hundred People Project' from Chinese Academy of Sciences and CAS-Shanghai Science Research Center (CAS-SSRC-YJ-2015-01). B.Z. is supported by the development fund for Shanghai talents, Shanghai Natural Science Foundation of China (16ZR443200) and National Natural science foundation of China (11604357). X.C.Z. is supported by a grant from Nebraska Center for Energy Sciences Research and a Qian-ren B (One Thousand Talent Plan B) summer research fund from USTC, and by a State Key R&D Fund of China (2016YFA0200604) to USTC. The computational resources utilized in this research were provided by Shanghai Supercomputer Center, National Supercomputing Center in Tianjin and Shenzhen, special programme for applied research on super computation of the NSFC-Guangdong joint fund (the second phase) and NC3 computer facility in University of Nebraska-Lincoln.

Author contributions

Y.G. created the idea and initiated the model. Y.G. and X.C.Z. designed the whole project. W.W.X., B.Z., X.C.Z. and Y.G. developed the model. X.C.Z. introduced flavour concept. W.W.X. performed all the calculations and plotted the pictures. W.W.X., B.Z., X.C.Z. and Y.G. wrote the manuscript. All authors discussed the results and commented on the manuscript.

Additional information

Supplementary Information accompanies this paper at http://www.nature.com/naturecommunications

Competing financial interests: The authors declare no competing financial interests.

Reprints and permission information is available online at http://npg.nature.com/reprintsandpermissions/

How to cite this article: Xu, W. W. *et al.* A grand unified model for liganded gold clusters. *Nat. Commun.* **7,** 13574 doi: 10.1038/ncomms13574 (2016).

Publisher's note: Springer Nature remains neutral with regard to jurisdictional claims in published maps and institutional affiliations.